Preparation of Nanoclay-Dispersed Polystyrene Nanofibers via Atom Transfer Radical Polymerization and Electrospinning

Hossein Roghani-Mamaqani,[1] Vahid Haddadi-Asl,[1] Mohammad Najafi,[1,2] Mehdi Salami-Kalajahi[1,2]

[1]*Department of Polymer Engineering and Color Technology, Amirkabir University of Technology, P. O. Box 15875-4413, Tehran, Iran*
[2]*Polymer Engineering Division, Research Institute of Petroleum Industry, 1485733111, Tehran, Iran*

Received 15 March 2010; accepted 29 July 2010
DOI 10.1002/app.33119
Published online 29 November 2010 in Wiley Online Library (wileyonlinelibrary.com).

ABSTRACT: In this study, clay-dispersed polystyrene (PS) nanocomposites were prepared with the *in situ* atom transfer radical polymerization method and were subsequently electrospun to form nanofibers 450–650 nm in diameter. The polymer chains extracted from the clay-dispersed nanofibers exhibited a narrow range of molecular weight distribution. Thermogravimetric analysis (TGA) confirmed a higher thermal stability of the resulting nanocomposites compared to PS. The effect of the weight ratio of montmorillonite on the thermal properties of the nanocomposites was also studied by TGA. Differential scanning calorimetry revealed that the addition of the nanoclay increased the glass-transition temperature. Moreover, degradation of the bromide chain-end functionality took place at low temperatures. Scanning electron microscopy showed that the average diameter of the fibers was around 500 nm. The dispersion of clay layers was also evaluated by Al atoms in the PS matrix with the energy-dispersive X-ray detection technique. Transmission electron microscopy confirmed the exfoliation of the nanoclay within the matrix. However, the clay layers were oriented along the nanofiber axis. © 2010 Wiley Periodicals, Inc. J Appl Polym Sci 120: 1431–1438, 2011

Key words: atom transfer radical polymerization (ATRP); gel permeation chromatography (GPC); morphology; nanocomposite; nanofiber

INTRODUCTION

Electrospun nanofibers have attracted great attention because they are used in a wide range of applications, such as scaffolds for tissue engineering,[1,2] sensors,[3] molecular electronics,[4] and protective clothing.[5] In this regard, electrospinning is known as a useful method for preparing nanowebs a few hundred nanometers in diameter. In addition, various polymers, polymer blends, sol–gels, and composites can be used in this method to produce nanofibers. Because nanowebs posses a high specific surface area and because their pore size are in the range of a few nanometers, it is easy to functionalize their surface. Therefore, they represent a wide range of physical and chemical properties. Through electrospinning, a filament is electrospun from a polymer solution[6,7] or a polymer melt in a high electric field.[8] Template synthesis was also commonly used in the past for the production of nanofibers; this method used a template with channels to introduce the precursor material.[9,10]

The incorporation of inorganic nanoclay layers into a polymer matrix enhances the electrical and mechanical properties, thermal stability, flame retardancy, gas permeation, and modulus of the neat polymer matrix.[11–15] These characteristics are mainly due to the high aspect ratio, nanometric thickness, and inorganic nature of the clay platelets. However, the degree of clay dispersion within the polymer matrix affects the nanocomposite structure and, consequently, the mentioned properties. On the basis of the reactants, processing systems, and interactions between clay layers and the host polymer, three major methods are used for the preparation of nanocomposites: melt intercalation, solution blending, and *in situ* polymerization.[16,17] *In situ* polymerization results in an exfoliated structure; this is due to the low viscosity of the monomer, which enables monomer–clay intercalation.

The synthesis of polymers with a narrow molecular weight distribution and predefined topologies by controlled radical polymerization (CRP) has been the subject of many studies in recent decades.[18,19] Mechanistically, CRP is based on an equilibrium reaction that quickly switches between active and dormant states to minimize the instantaneous concentration of free

Correspondence to: V. Haddadi-Asl (haddadi@aut.ac.ir).
Contract grant sponsor: Iran Petrochemical Research and Technology Co.; contract grant number: 0870128706.

radicals and, therefore, to suppress irreversible bimolecular reactions. In this study, nitroxide-mediated polymerization,[20,21] reversible addition–fragmentation chain transfer polymerization (RAFT),[22,23] and atom transfer radical polymerization (ATRP)[24,25] were thoroughly studied. The main advantages of ATRP systems over CRP systems are their applicability in a wide range of monomers and polymerization systems (its equilibrium can be easily adjusted for a given system by modification of the ligand of the catalyst),[26] the simplicity of the reaction setup and conditions (low temperature and pressure), and the lower sensitivity to impurities.[27]

According to the literature, a number of attempts have been made to produce nanocomposites via CRP methods. Different polymer nanocomposites with narrow molecular weight distributions have been synthesized by nitroxide-mediated polymerization,[28] RAFT,[29] and ATRP.[30–33] Because the monomer penetrates an intergallery of clay platelets and because polymerization is initiated under appropriate conditions, the silicate layers may be gradually pushed apart, and a well-dispersed exfoliated structure may result. Fu et al.[34] combined the electrospinning, ATRP, and RAFT methods to produce smart nanofibers and obtained poly(vinylbenzyl chloride-*co*-glycidyl methacrylate) nanofibers 0.4–1.5 μm in diameter. The spinning of core–sheath nanofibers by ATRP and electrospinning was also studied by Fu et al.[35] They produced polystyrene (PS) nanofibers 10–1000 nm in diameter. Subsequently, PS nanofibers were used as a core for the surface initiation of acrylamide sheaths. The effect of the solvent on the preparation of styrene nanofibers was studied by Uyar and Besenbacher.[36] They reported that the reproducibility of uniform PS fibers by electrospinning was greatly dependent on the solution conductivity. The electrospinning of different polymers in the presence of nanoclay has also been investigated extensively. Wang et al.[37] studied the use of montmorillonite to enhance the thermal properties of electrospun nanofibers of methyl methacrylate and methacrylic acid copolymer (poly(MMA-co-MAA)). They found out that dispersion of clay within the nanocomposites improved the electrospinnability of the nanocomposites. Polyurethane nanocomposite nanofibers were prepared with electrospinning by Hong et al.[38] They also reported that exfoliated clay layers oriented along the fibers. However, no one has reported an attempt to prepare tailor-made PS nanocomposite nanofibers. An exfoliated PS nanocomposite may be an appropriate resource of clay-dispersed PS nanofibers.

In this study, ATRP was used to synthesize well-defined PS nanocomposites; then, the clay-dispersed PS was used as a precursor to prepare PS nanocomposite nanofibers. At first, ATRP was applied to a mixture of monomer and Cloisite 30B. The platelets of nanoclay were pushed apart as the ATRP process continued. Consequently, PS chains with a narrow molecular weight distribution in the vicinity of the nanoclay platelets resulted. Finally, nanoclay-loaded PS nanofibers were obtained by the electrospinning of the nanocomposite solution with the mixed xylene and tetrahydrofuran (THF) method.

EXPERIMENTAL

Materials

Styrene (Aldrich, Milwaukee, WI, 99%) was passed through an alumina-filled column, dried over calcium hydride, and then distilled under reduced pressure (60°C, 40 mmHg). Cloisite 30B, a montmorillonite treated by an ion-exchanged reaction with the surfactant methyl tallow bis-2-hydroxy ethyl quaternary ammonium (Southern Clay Products, Gonzales, TX), was stored in a vacuum oven (60°C, 40 mmHg) before use. Copper(I) bromide (CuBr; Aldrich, Milwaukee, WI, 98%) was washed by glacial acetic acid, filtered, washed again by ethanol, dried in a vacuum oven (50°C, 40 mmHg), and then stored under a nitrogen blanket. *N,N,N′,N″,N″*-pentamethyldiethylenetriamine (PMDETA; Aldrich, Milwaukee, WI, 99%), ethyl α-bromoisobutyrate (EBiB; Aldrich, Milwaukee, WI, 97%), anisole (Aldrich, Milwaukee, WI, 99%), and neutral aluminum oxide (Aldrich, Milwaukee, WI) were used as received.

Preparation of the PS/clay nanocomposites

The ATRP polymerizations were performed in a 250-mL laboratory reactor, which was placed in an oil bath thermostated at the desired temperature. A number of batch polymerizations were run at 110°C in the bulk with a molar ratio of 200 : 1 : 1 : 1 for [Monomer] : [EBiB] : [CuBr] : [PMDETA], to give a theoretical polymer molecular weight of 20,830 g/mol at 100% conversion. The reactor was degassed and back-filled with nitrogen gas three times and then kept under N_2. We ran the batch experiments by adding the deoxygenated monomer (styrene, 23.040 mL, 0.02 mol), Cloisite 30B, the catalyst (CuBr, 0.287 g, 0.002 mol), the ligand (PMDETA, 0.417 mL, 0.002 mol), and 0.50 mL of deoxygenated anisole as an internal standard in an orderly fashion to the reactor and then increasing the reaction temperature up to 110°C (for ~15 min). The solution turned a light green as the CuBr/PMDETA complex formed. Finally, after the formation of the metal complex, the initiator (EBiB, 0.293 mL, 0.002 mol) was added to the system to start the styrene ATRP. A sample was taken before the reaction started and was used as a reference for the samples taken later,

TABLE I
Designation of the Samples and Various Modes of Their Preparation with the Contents of the Nanoclay

Sample designation	Method of preparation	Proportion of clay (wt %)	Duration of the monomer and clay dispersion (h)
PS	ATRP	0	–
PSN220	*In situ* ATRP	2	20
PSN420	*In situ* ATRP	4	20
PSN1020	*In situ* ATRP	10	20

at different stages of the reaction, to measure the extent of monomer conversion.

Separation of the polymer chains from the clay

The polymer samples were dissolved in THF and passed through a neutral aluminum oxide column to remove catalyst particles. With high-speed ultracentrifugation and then passage of the solution through a 0.2-μm filter, the PS chains were separated from the clay platelets.[39]

Electrospinning of the PS nanocomposites

The PS nanocomposites containing 4 wt % nanoclay (with respect to monomer) were used for nanofiber fabrication. The 40 wt % solutions of the nanocomposites were prepared by dissolution of the nanocomposite in a mixed solvent of xylene and THF (2/1 w/w) after 12 h of vigorous mixing. A 10-mL disposable syringe was used to stock each of the prepared solutions. A syringe pump was used to feed the solution at a constant flow rate of 1 mL/h. To collect nanofibers, a cylindrical stainless steel collector was located a fixed distance from the needle. A high voltage of 15 kV was applied between the needle and the collector, and the setup was operated at 25°C.

The designation of the samples and various modes of their preparation with the content of nanoclay are summarized in Table I.

Analysis

The average molecular weights and molecular weight distributions were measured by the gel permeation chromatography (GPC) technique. To this end, a Waters 2000 ALLIANCE (Milford, MA) with a set of three columns with pore sizes of 10,000, 1000, and 500 Å was used. THF was used as the eluent at a flow rate of 1.0 mL/min, and the calibration was carried out with narrow-molecular-weight-distribution PS standards. For the GPC measurements, we removed the catalyst particles by passing the polymer solutions through a neutral aluminum oxide column. Thermal analyses were carried out with a differential scanning calorimetry (DSC) instrument (NETZSCH DSC 200 F3, Netzsch Co, Selb/Bavaria, Germany). Nitrogen was used as the purging gas at a rate of 50 mL/min. Aluminum pans containing 2–3 mg of the samples were sealed with the DSC sample press. The samples were heated from ambient temperature to 220°C at a constant heating rate of 10°C/min. The glass-transition temperature (T_g) was obtained at the inflection point of the heat capacity jump. Thermogravimetric analyses (TGAs) were carried out with a PL thermogravimetric analyzer (Polymer Laboratories; Loughborough, UK). The thermograms were obtained from ambient temperature to 550°C at a heating rate of 10°C/min. A sample weight of about 10 mg was used for all of the measurements, and nitrogen was used as the purging gas at the flow rate of 50 mL/min; an empty pan was used as the reference. A Vega Scanning electron microscope (Tescan, Czech Republic) equipped with an energy-dispersive X-ray spectroscopy (EDX) analyzer was used to evaluate the morphology of the nanofibers, which were gold-coated with a sputtering coater. A Philips transmission electron microscope (Model EM 208, Netherland) with an accelerating voltage of 200 kV was used to study the morphology of the nanocomposites. Samples 70 nm in thickness were prepared by a OMU-3 ultramicrotome (Reichert, Vienna, Austria).

RESULTS AND DISCUSSION

A nanoclay with an intercalating agent containing two hydroxyl groups, Cloisite 30B, was used to prepare the PS nanocomposites through the *in situ* ATRP method.

Figure 1 shows the number- and weight-average molecular weights and polydispersity indices (PDIs) of the resultant polymers. The GPC traces of all of the samples represented monomodal peaks

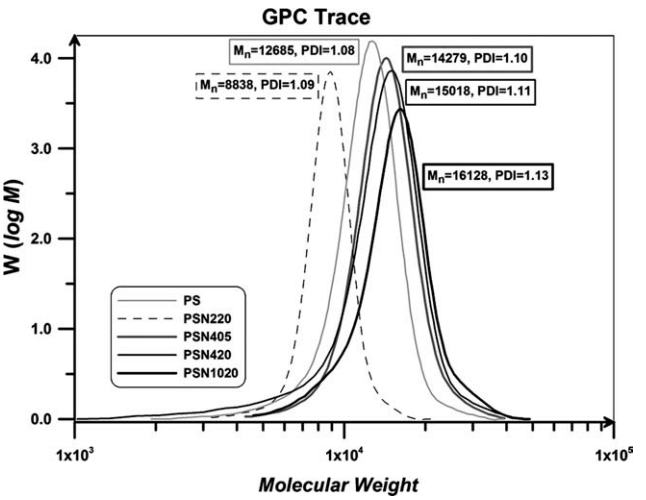

Figure 1 GPC traces of the PS macroinitiator and nanocomposites prepared via ATRP with their number average molecular weight (M_w) and polydispersity index (PDI).

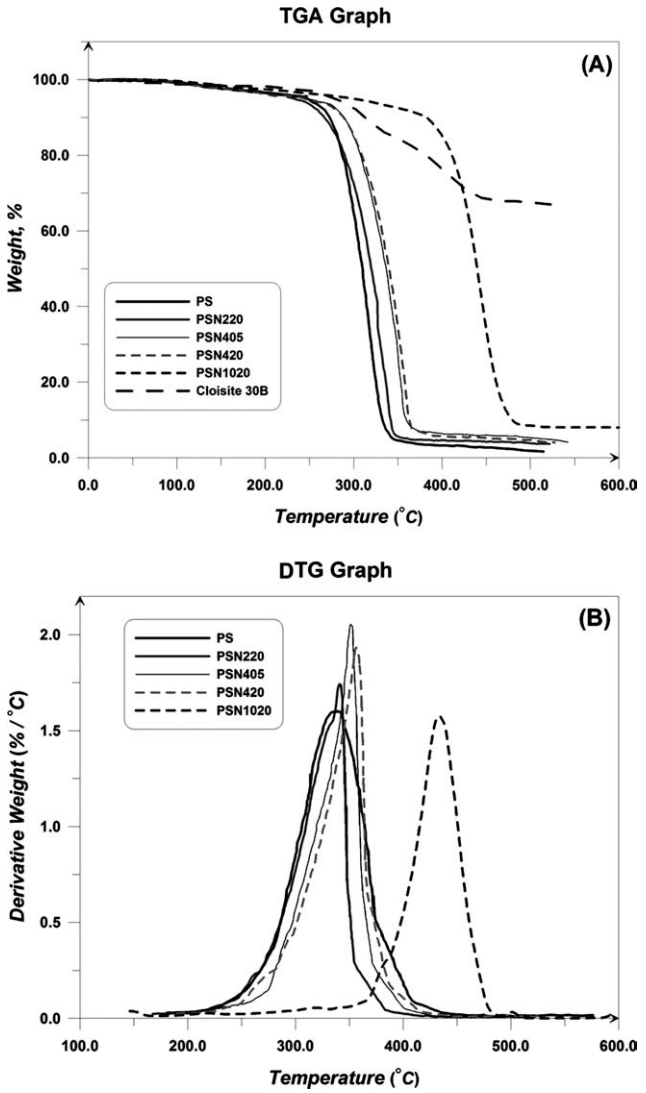

Figure 2 (A) TGA and (B) DTG thermograms of PS and its nanocomposites with different clay contents.

corresponding to the molecular weight values predetermined by the molar ratio of the monomer to the initiator. Increasing the clay content resulted in a rise in the molecular weight and, consequently, the rate of polymerization; this was attributed to the pendant hydroxyl group of the modifier attached to the clay surface. This partially polarized the reaction medium and, thereby, exerted an acceleration effect on the polymerization rate. As reported previously, polar solvents (especially hydroxyl containing ones, e.g., water, phenol, and carboxylic acids) exerted a rate acceleration effect on the polymerization systems by increasing the radical activation rate and reducing the radical recombination rate.[40,41] Pendant hydroxyl groups of the clay layers may possibly have caused a polarity change into the reaction medium. Additionally, it is evident from recent research that a negatively charged surface (pendant hydroxyl groups of clay layers in this study) could absorb and hold a positively charged catalyst (Cu ions) and, consequently, increase the rate of chain growth.[42] The high values of initiator efficiency also signify the controlled nature of the polymerization and, additionally, the accelerating effect of a nanoclay on the polymerization rate in styrene ATRP. The accelerating effect of nanoclays on the polymerization rate has also been reported in other studies.[32,33] The PDI of the polymer chains increased with the addition of the nanoclay. The addition of the nanoclay (which acted as an impurity in the polymerization system) broadened the molecular weight distribution of the resulting polymers. The PDI value increased from 1.08 to 1.13 with the addition of 10 wt % nanoclay. However, the initiator efficiency decreased from 0.94 to 0.89. The effect of the nanoclay swelling time before polymerization was also studied by the comparison of the PSN405 and PSN420 samples (see Table I for descriptions of the samples). The lower initiator efficiency and higher PDI values obtained in PSN420 showed that longer swelling times resulted in a higher diffusion of monomer into the interlayer of the clay platelets and, thereby, magnified the effect of the polarity change. Consequently, a higher rate of polymerization and a higher molecular weight were achieved at a similar reaction time compared to the PSN405 sample.

The thermal stability of the specimens was studied by TGA. Figure 2(A) illustrates typical TGA thermograms of weight loss as a function of temperature at 50–550°C for the neat PS and the nanocomposites. As shown, the thermal stability of all of the nanocomposites was higher than that of the neat PS. When the clay content of the nanocomposites was increased, the degradation temperature increased. The 32% weight loss of the Cloisite 30B thermogram (up to 500°C) was attributed to its ammonium salt modifier degradation, and the remaining portion (char) included inorganic contents. Figure 2(B) shows the corresponding differential thermogravimetric (DTG) curves of PS and its nanocomposites at different clay contents. It is clear that the addition of clay nanolayers to PS retarded its degradation. This

TABLE II
Thermal Properties of PS and Its Nanocomposites with Different Clay Loadings

Sample designation	TGA				DTG peak	
	$T_{0.05}$	$T_{0.1}$	$T_{0.5}$	Char (%)	Start (°C)	End (°C)
PS	239	267	311	1.8	177	438
PSN220	242	275	320	3.8	210	447
PSN420	246	288	339	5.7	215	451
PSN405	245	288	336	5.7	213	451
PSN1020	279	382	439	10.7	341	494

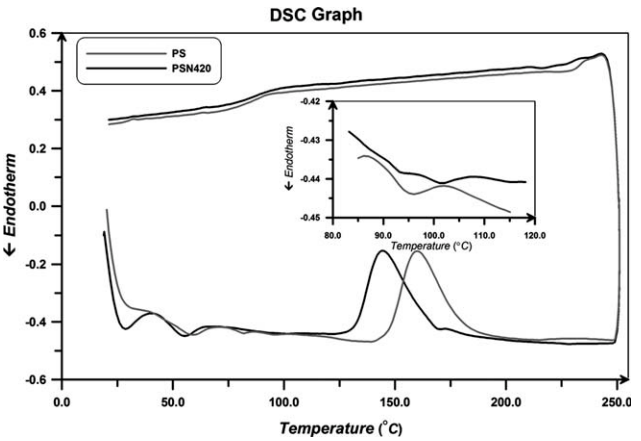

Figure 3 DSC thermogram of PS and PSN420.

was attributed to the hindrance effect of nanoplatelets on the mobility of polymer chains.

The TGA data summarized in Table II show the temperature thresholds of $T_{0.05}$, $T_{0.1}$, and $T_{0.5}$ at which 5, 10, and 50% of the polymer degradation occurred. It is obvious that the degradation temperature was lower for smaller clay contents and rose at higher contents. Additionally, the amount of char, as listed in Table II, increased as the percentage of clay increased. The degradation of all of the samples took place in one step, and char remained after complete degradation. The degradation of neat PS occurred in the temperature range 170–438°C. However, the nanocomposite samples exhibited a temperature window of 200–450°C for degradation. The effect of the dispersion time of clay in the monomer before polymerization could also be studied at temperatures at which a certain percentage of degradation occurred.

TABLE III
T_g Values, the C—Br Degradation Temperature, and Required Energy Values in PS and Its Nanocomposites

Sample designation	Molecular weight (g/mol)	T_g (°C)	T_d (°C)	ΔH_d (J/g)
PS	11,615	90.2	159.9	41.31
PSN420	15,018	92.1	144.5	39.96
PSN1020	16,128	95.2	138.7	35.59
Anionic[43]	15,020	93	–	–

The PSN420 sample (swelling time = 20 h) displayed a slightly higher degradation temperature. The solution blending specimen, because of its nonexfoliated morphology, showed poor thermal properties compared to the samples with the same clay content prepared via the *in situ* polymerization method.

The confinement effect of the nanolayers on the mobility of the PS chains was evaluated by comparison of the T_g values of the neat PS and the clay-loaded PS nanocomposites with a differential scanning calorimeter. Figure 3 illustrates the thermal behavior of PS and PSN420. A temperature window of 20–240°C was used to analyze the DSC results. The clay layers experienced no transition, and therefore, only thermal transitions of PS chains were observed. Apart from the initial instability, an inflection and a peak were observed in the heating procedure. The temperature of inflection was the same as T_g. Nevertheless, no peak was observed during the cooling path; this indicated that samples did not undergo melting or other reversible thermal transformations. Thus, the exothermic peak was due to

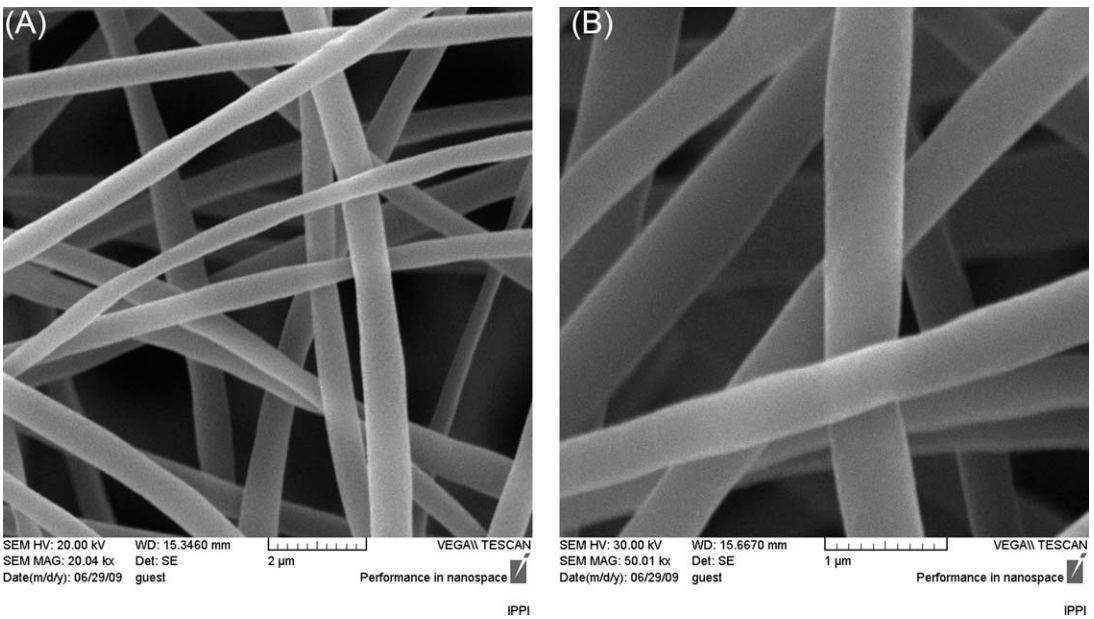

Figure 4 SEM images of PSN420 at two different magnifications.

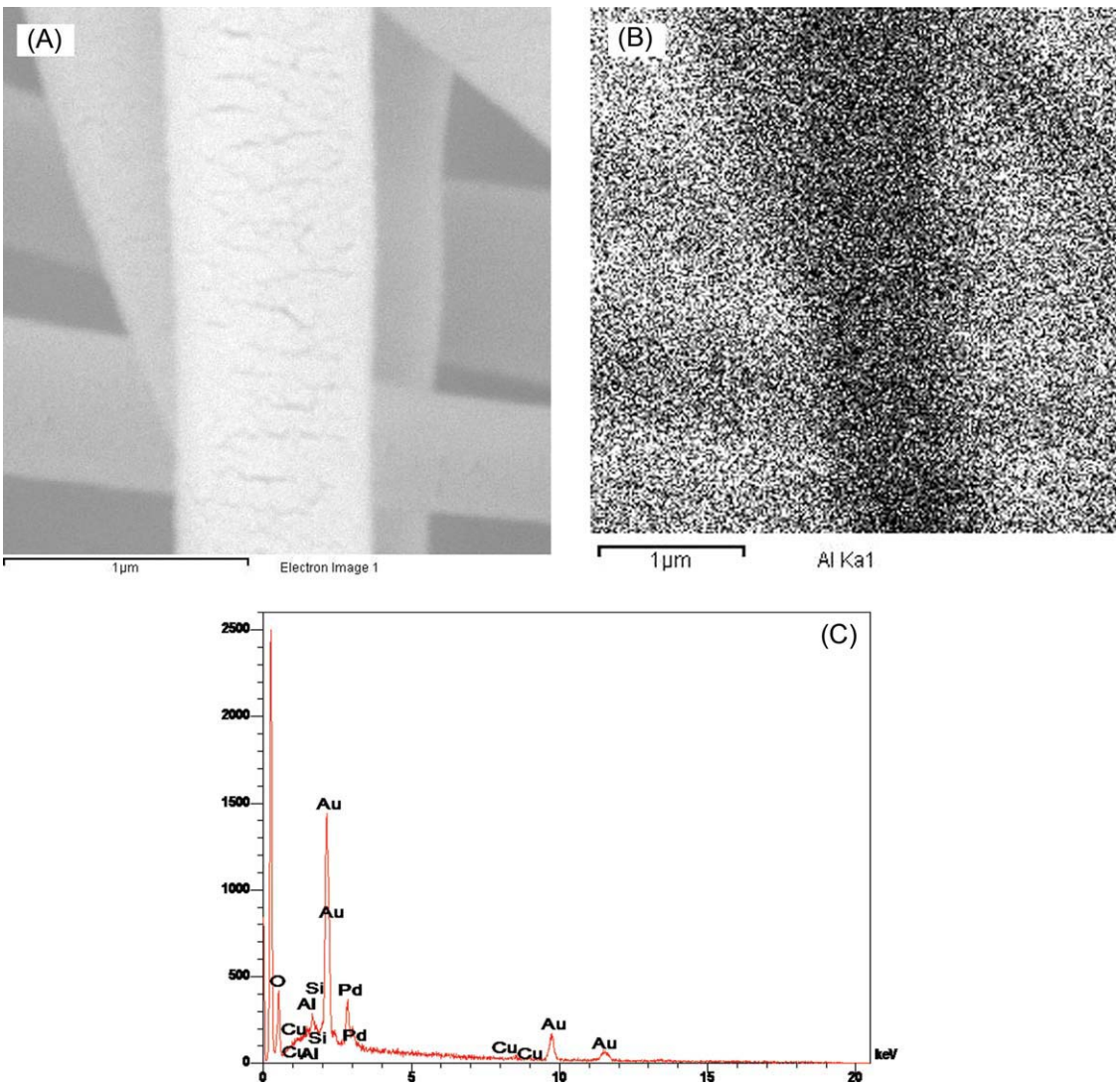

Figure 5 (A) SEM image, (B) aluminum distribution pattern, and (C) EDX spectrum of PSN420. [Color figure can be viewed in the online issue, which is available at wileyonlinelibrary.com.]

the cleavage of the C—Br bond. The temperature at which C—Br bond cleavage occurred demonstrated the catalytic effect of the nanoclay layers in ATRP.

Table III summarizes the C—Br dissociation energy (ΔH_d), the C—Br cleavage temperature (T_d), and also, the T_g values of PS and its nanocomposites. An anionic PS[43] was used to compare the ATRP synthesis results. Anionic polymerization, similar to ATRP, resulted in polymer chains with narrow molecular weight distributions; therefore, it appeared that these two methods resulted in polymers with similar T_g values, provided that they had the same molecular weight. At higher clay contents, the T_g increased; this was the result of a nanoclay confinement effect on the mobility of the PS chains. Generally, a higher clay content means higher C—Br cleavage; this is due to conductivity of nanoclay platelets.

The scanning electron microscopy (SEM) images of the PSN420 nanofibers prepared by electrospinning are depicted in Figure 4. The morphology and average diameter can easily be observed in this figure. Fibers with an average diameter of 450–650 nm were obtained by this process. The molecular weight of the PSN420 PS chains was low, and the optimum conditions for its electrospinning are described in the Experimental section. The smallest variations in the accelerating voltage, solution flow rate, and distance between the needle and collector resulted in instability of the nanofiber morphology and fibers with uneven diameters.

EDX was used to investigate the dispersion of nanoclay in the nanofiber matrix by the detection of the aluminum atoms of the nanoclay. The EDX image and its corresponding SEM micrograph [Fig. 5(A)] showed the distribution pattern of aluminum within the nanofibers. The other characteristic atoms of nanoclay, namely, silica and oxygen, were studied in detail with the EDX spectra [Fig. 5(C)].

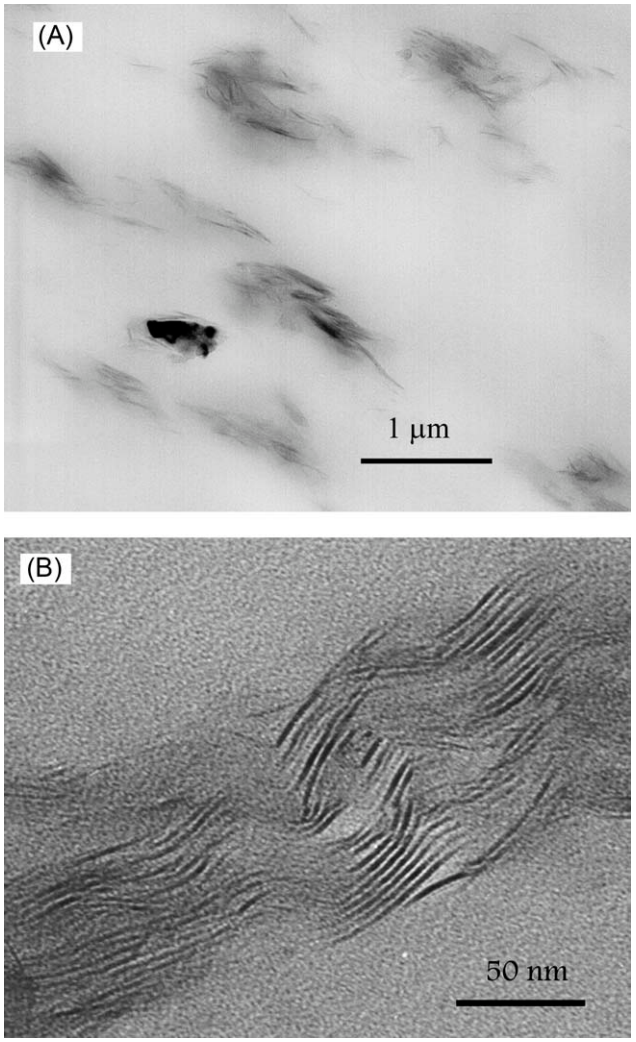

Figure 6 TEM image of PSN420 with magnifications of (A) 1 μm and (B) 50 nm.

The transmission electron microscopy (TEM) images shown in Figure 6 were used to study the delamination and dispersion of clay platelets in the matrix. The TEM images confirmed the exfoliation of clay layers in the matrix nanocomposite containing 4 wt % nanoclay. The exfoliated clay platelets are specified by the tactoids in Figure 6(A). The light and dark areas represent the PS matrix and silicate layers, respectively. The interlayer expansion and disorderly dispersed clay layers clearly indicated the exfoliation of clay layers with the polymer chains. The lack of space between the clay platelets and polymer matrix confirmed that Cloisite 30B was compatible with the PS matrix because of the presence of the two hydroxyl groups on the ammonium salt structure. Figure 6(B) shows the ordered structure of the nanoclay platelets in the nanofiber; this was due to the longitudinal rearrangement of nanolayers along the length of the fibers.

CONCLUSIONS

PS and its nanocomposites, which contained different clay contents, were synthesized by ATRP. Subsequently, the nanocomposite containing 4 wt % nanoclay was electrospun to form fibers with diameters in the submicrometer range. The controlled nature of ATRP facilitates the synthesis of tailor-made nanocomposites with a predictable degree of polymerization. The GPC traces of all of the samples represented a monomodal peak, and the PDI of the polymer chains increased with the addition of the nanoclay. The nanocomposites had a higher molecular weight and a broader molecular weight distribution. The thermal stabilities of all of the nanocomposites were higher than that of the neat PS. When the clay content of the nanocomposites was increased, the degradation temperature increased. The longer the swelling time was, the more the degradation temperature increased. No peaks were observed during the DSC cooling path; this indicated that the samples had not undergone melting or other reversible thermal transformations. The exothermic DSC peak was a result of C—Br bond cleavage. The higher percentage of nanoclay increased the T_g values of the samples; this was due to the confinement effect of nanoclay. According to the SEM images, the average diameter of the nanofibers was in the range 450–650 nm. The distribution of specific atoms, such as Al, Si, and O, was studied by EDX imaging. The TEM results indicate that the clay layers were exfoliated in the PS matrix of the PSN420 nanofibers; however, the nanoclay platelets were oriented along the length of the nanofibers.

References

1. Jin, H. J.; Fridrikh, S. V.; Rutledge, G. C.; Kaplan, D. L. Biomacromolecules 2002, 3, 1233.
2. Matthews, J. A.; Wnek, G. E.; Simpson, D. G.; Bowlin, G. L. Biomacromolecules 2002, 3, 232.
3. Wang, X. Y.; Drew, C.; Lee, S. H. J Macromol Sci Pure Appl Chem 2002, 39, 1251.
4. Norris, I. D.; Shaker, M. M.; Ko, F. K.; MacDiarmid A. G. Synth Met 2000, 114, 109.
5. Gibson, P. W.; Schreuder-Gibson, H. L.; Rivin, D. AIChE J 1999, 45, 190.
6. Li, D.; Xia, Y. N. Adv Mater 2004, 16, 1151.
7. Huang, Z. M.; Zhang, Y. Z.; Kotaki, M.; Ramakrishna, S. Compos Sci Technol 2003, 63, 2223.
8. Dalton, P. D.; Grafahrend, D.; Klinkhammer, K.; Klee, D.; Moller, M. Polymer 2007, 48, 6823.
9. Han, Y. J.; Kim, J. M.; Stucky, G. D. Chem Mater 2000, 12, 2068.
10. Xu, D.; Chen, D.; Guo, G.; Gui, L.; Tang, Y. Adv Mater 2000, 11, 520.
11. Fujimori, A.; Ninomiya, N.; Masuko, T. Polym Adv Technol 2008, 19, 1735.
12. Jang, B. N.; Costache, M.; Wilkie, C. A. Polymer 2005, 46, 10678.
13. Caruso, F.; Spasova, M.; Susha, A.; Giersig, H.; Caruso, R. A. Chem Mater 2001, 13, 109.

14. Nazarenko, S.; Meneghetti, P.; Julmon, P.; Olson, B.; Qutubuddin, S. J Polym Sci Part B: Polym Phys 2007, 45, 1733.
15. Shia, D.; Hui, C. Y.; Burnside, S. D.; Giannelis, E. P. Polym Compos 1998, 19, 608.
16. Akelah, A.; Moet, A. J Mater Sci 1996, 31, 3589.
17. Fu, X.; Qutubuddin, S. Polymer 2001, 42, 807.
18. Cunningham, M. F. Prog Polym Sci 2002, 27, 1039.
19. Qui, J.; Charleux, B.; Matyjaszewski, K. Prog Polym Sci 2001, 26, 2083.
20. Georges, M. K.; Veregin, R. P. N.; Kazmaier, P. M.; Hamer, G. K. Macromolecules 1993, 26, 2987.
21. Benoit, D.; Chaplinski, V.; Braslau, R.; Hawker, C. J. J Am Chem Soc 1999, 121, 3904.
22. Chiefari, J.; Chong, Y. K.; Ercole, F.; Krstina, J.; Jeffery, J.; Le, T. P. T.; Mayadunne, R. T. A.; Meijs, G. F.; Moad, C. L.; Moad, G.; Rizzardo, E.; Thang, S. H. Macromolecules 1998, 31, 5559.
23. Chong, Y. K.; Le, T. P. T.; Moad, G.; Rizzardo, E.; Thang, S. H. Macromolecules 1999, 32, 2071.
24. Najafi, M.; Haddadi-Asl, V.; Salami-Kalajahi, M.; Roghani-Mamaqani, H. e-Polymers 2009, 030.
25. Najafi, M.; Roghani-Mamaqani, H.; Salami-Kalajahi, M.; Haddadi-Asl, V. Chin J Polym Sci 2010, 28, 483.
26. Matyjaszewski, K.; Xia, J. Chem Rev 2001, 101, 2921.
27. Jakubowski, W.; Matyjaszewski, K. Angew Chem 2006, 118, 4594.
28. Schmid, A.; Fujii, S.; Armes, S. P. Langmuir 2006, 22, 4923.
29. Salem, N.; Shipp, D. A. Polymer 2005, 46, 8573.
30. Roghani-Mamaqani, H.; Haddadi-Asl, V.; Najafi, M.; Salami-Kalajahi, M. Polym Compos, to appear.
31. Haimanti, D.; Nikhil, S.; Anil, B. J Appl Polym Sci 2008, 108, 2398.
32. Haimanti, D.; Nikhil, S.; Anil, B. Macromolecules 2008, 41, 50.
33. Roghani-Mamaqani, H.; Haddadi-Asl, V.; Najafi, M.; Salami-Kalajahi, M. AIChE J, to appear.
34. Fu, G. D.; Xu, L. Q.; Yao, F.; Zhang, K.; Wang, X. F.; Zhu, M. F.; Nie, S. Z. Appl Mater Interfaces 2009, 1, 239.
35. Fu, G. D.; Lei, J. Y.; Yao, C.; Li, X. S.; Yao, F. Macromolecules 2008, 41, 6854.
36. Uyar, T.; Besenbacher, F. Polymer 2008, 49, 5336.
37. Wang, M.; Hsieh, A. J.; Rutledge, G. C. Polymer 2005, 46, 3407.
38. Hong, J. H.; Jeong, E. H.; Lee, H. S.; Baik, D. H.; Seo, S. W.; Youk, J. H. J Polym Sci Part B: Polym Phys 2005, 43, 3171.
39. Akelah, A.; Rehab, A.; Agag, T.; Betiha, M. J Appl Polym Sci 2007, 103, 3739.
40. Wang, X. S.; Armes, S. P. Macromolecules 2000, 33, 6640.
41. Haddleton, D. M.; Heming, A. M.; Kukulji, D.; Duncalf, D. J.; Shooter, A. J. Macromolecules 1998, 31, 2016.
42. Kizhakkedathu, J. N.; Brooks, D. E. Macromolecules 2003, 36, 591.
43. Savin, D. A.; Pyun, J.; Patterson, G. D.; Kowalewski, T.; Matyjaszewski, K. J Polym Sci Part B: Polym Phys 2002, 40, 2667.